

Stress analysis of a new steel-concrete composite I-girder

Yamin Wang and Yongbo Shao*

School of Civil Engineering and Architecture, Southwest Petroleum University, Chengdu, 610500, PR China

(Received July 1, 2017, Revised April 11, 2018, Accepted April 17, 2018)

Abstract. A new I-girder consisted of top concrete-filled tubular flange and corrugated web has been proved to have high resistance to both global buckling of the entire girder and local buckling of the web. This study carries out theoretical analysis and experimental tests for this new I-girder to investigate the stress distribution in the flanges and in the corrugated web. Based on some reasonable assumptions, theoretical equations for calculating the normal stress in the flanges and the shear stress in the corrugated web are presented. To verify the accuracy of the presented equations, experimental tests on two specimens were carried out, and the experimental results of stress distribution were used to assess the theoretical prediction. Comparison between the two results indicates that the presented theoretical equations have enough accuracy for calculating the stress in the new I-girder, and thus they can be used reliably in the design stage.

Keywords: I-girder; concrete-filled tubular flange; corrugated web; stress distribution; theoretical equations

1. Introduction

Steel I-girder is widely used in building and bridge engineering. A conventional I-girder is consisted of two flat-plate flanges and a flat-plate web. In a bridge with a large span, the height of the I-girder is generally high for providing high flexural strength and stiffness. However, a large height is disadvantageous for global stability. Simultaneously, the flat-plate web is sensitive to local buckling because its large height-to-width ratio. To improve the resistance of an I-girder to global buckling, the flat-plate flange under compression was suggested to be designed as a tubular shape (namely hollow flange). Pi and Trahair (1997) presented a triangular hollow flange beam (THFB) as shown in Fig. 1(a). A cold-formed steel C-shape section with rectangular hollow flanges, as shown in Fig. 1(b), was presented by Zhao and Mahendran (1998). This C-shape beam or girder is also called Lite Steel Beam (LSB). Hassanein and Kharoob (2010) studied a rectangular hollow tubular flange plate girder (RHTFPG) as shown in Fig. 1(c). The hollow tubular flange has much higher torsional stiffness compared to a flat-plate due to its closed section, and the resistance to global buckling for an I-girder with hollow tubular flange is hence expected to be improved greatly.

However, two typical failure modes, i.e., web distortion and local buckling, are very common in a hollow flange due to its thin-walled attribution (Anapayan *et al.* 2011, Hassanein and Silvestre 2013). Web distortion occurs when the flat-plate web has a larger slenderness, and it can be

avoided efficiently by placing stiffeners (Avery and Mahendran 1997, Mahendran and Avery 1997, Hassanein *et al.* 2013). To avoid the local buckling of the thin-walled tubular flange, concrete is infilled to form a concrete-filled tubular flange as shown in Fig. 2. The global stability of an I-girder with concrete-filled tubular flange was proved to be improved greatly through both experimental tests and finite element analyses (Kim *et al.* 2005, Kim and Sause 2008, Sause *et al.* 2008, Gao *et al.* 2014). The advantages of I-girders with concrete-filled tubular flange are very challenging in the application in bridge engineering due to their high capacity to resisting global buckling (Sause 2015).

As mentioned above, stiffeners are generally placed on the web to avoid web buckling in an I-girder with a large height. The stiffeners are welded symmetrically onto the web surface. As the I-girder used in bridge engineering is always subjected to cyclic loading during service time, fatigue failure has to be considered. It is well known that fatigue failure is very sensitive in welding region and fatigue cracks initiate at the weld toe in most cases. Hence, welding stiffeners onto the web surface is not favorable for the fatigue strength. Corrugated plate was then presented to replace a flat-plate web to increase the out-of-plane flexural stiffness, and further to improve the resistance of the web to local buckling. The shear strength of steel beams with trapezoidally corrugated webs was studied by many researchers in the literature (Elgaaly *et al.* 1996, Sause and Braxtan 2011, Barakat *et al.* 2015). Through investigation on bending behavior of I-girders with corrugated webs, it was found that the corrugated web has very slight in-plane tensile or compressive stiffness. The moment was almost sustained by the flanges alone and the shear force was undertaken by the corrugated web (Abbas *et al.* 2006, Elgaaly *et al.* 1997, He *et al.* 2014, Chen *et al.* 2015). Kalali *et al.* (2015) introduced the application of corrugated plates

*Corresponding author, Ph.D., Professor,
E-mail: cybshao2009@hotmail.com;
ybshao@swpu.edu.cn

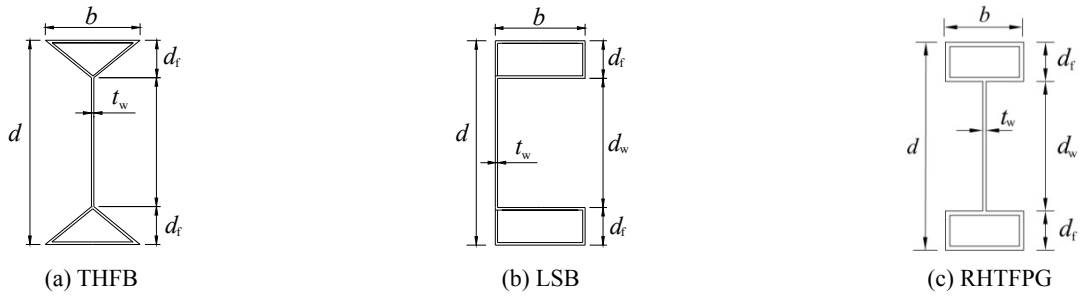


Fig. 1 I-girders with hollow flanges

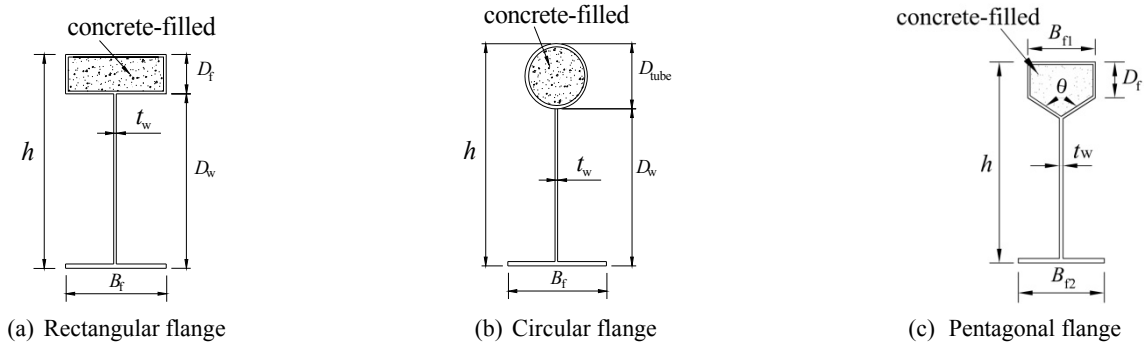


Fig. 2 Girders with concrete-filled tubular flanges

in steel plate shear walls (SPSWs) to lower the high construction cost. A numerical investigation of the hysteretic performance indicated that the cyclic response and energy absorption capacity of SPSWs with trapezoidally corrugated infill plates were improved greatly. Abbas *et al.* (2007a, b) and Kovesdi *et al.* (2012) presented theoretical method for calculating the stress distribution in an I-girder with corrugated web, and it was found that the normal stress in the flanges was consisted of in-plane component and transverse component. The latter normal stress was produced due to a transverse bending moment caused by the web corrugation.

A new I-girder consisted of concrete-filled tubular flange and corrugated web was presented by Shao and Wang (2016, 2017). The new I-girder was proved to have high resistance to both global buckling and local buckling. For design purpose, this study is furthered to present theoretical analysis for the stress distribution in this new I-girder.

2. Stress distribution in the new I-girder

2.1 General

The new I-girder presented by Shao and Wang (2016, 2017) is illustrated in Fig. 3. The I-girder is consisted of a top concrete-filled tubular flange, a bottom flat-plate flange and a corrugated web. This I-girder is suitable to be hinged at two ends and subjected to external loading on the top flange, which is a very common case in bridge engineering. The top concrete-filled tubular flange is under compression when the I-girder is under bending, and it has high capacity to resist lateral-distorsional deformation at global buckling. A rectangular tube in the top flange is used because it is more convenient compared to circular, triangular or pentagonal tube to connect the corrugated web to the top flange through welding. The corrugation is assumed to be trapezoidal.

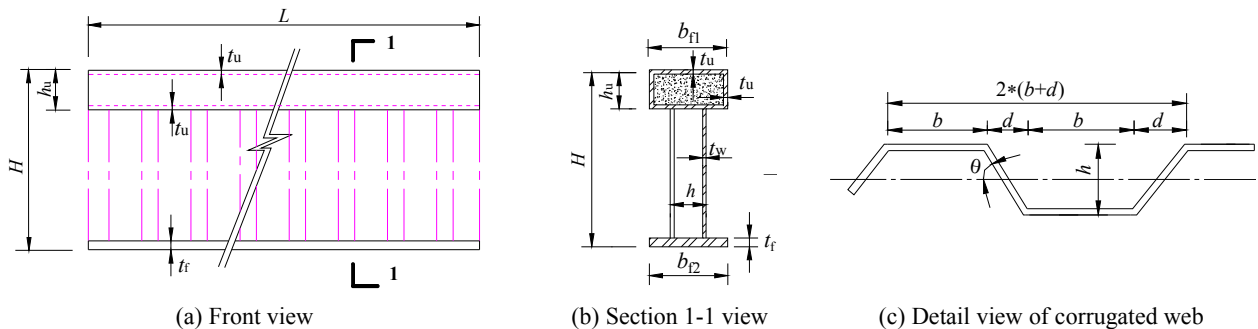


Fig. 3 Geometry of presented new I-girder

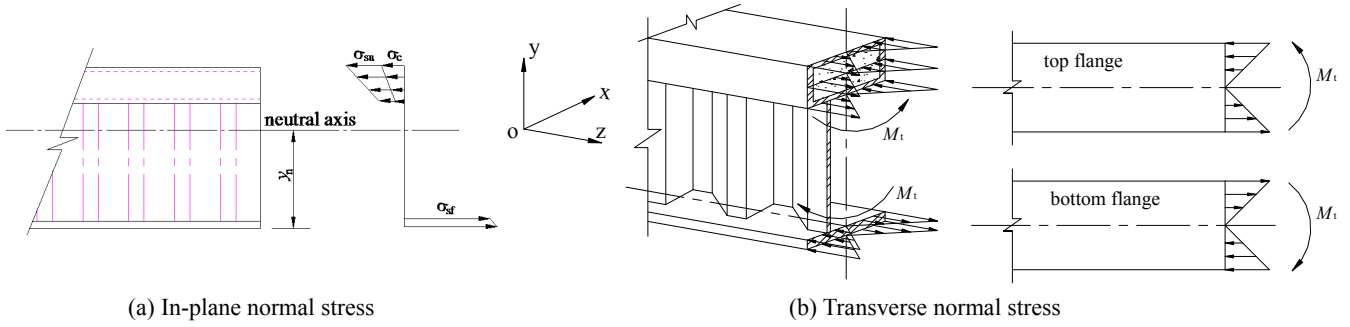


Fig. 4 Normal stress distribution in flanges

To carry out theoretical analysis for stress distribution in the presented new I-girder, some assumptions are given as follows:

- (1) The I-girder is assumed to be in linear and elastic state when it is subjected to external loading. Nonlinear and plastic state is not considered, i.e., limit state analysis for the I-girder is not considered in this study;
- (2) Plane assumption is still satisfied for the new I-girder, which indicates that the strain distribution along the height on the cross section is linear;
- (3) There is no separation between the steel tube and the infilled concrete in the top flange, and the concrete and the steel tube can cooperate together. This assumption is based on that shear stress is very minor in the flange because most of such component is sustained by the corrugated web. This assumption is reasonable in linear and elastic stress analysis;
- (4) The bending moment is only sustained by the two flanges, and the corrugated web has no contribution to sustain tension or compression;
- (5) The shear stress in the bottom flat-plate flange is negligible, i.e., the bottom flat-plate has only contribution to normal stress;
- (6) Reasonable design for the I-girder is assumed, and the neutral axis is located in the corrugated web. It is noted that the neutral axis may move to the flange at ultimate limit state. However, a reasonable design for the cross section in linear and elastic stage is to locate the neutral axis in the web.

2.2 Normal stress in the flanges

According to the assumption (4) in the above session,

normal stress only exists in the two flanges. Both in-plane normal stress and transverse normal stress are produced in the flanges when the I-girder is subjected to in-plane bending load, as shown in Fig. 4. The in-plane normal stress is produced due to the in-plane bending moment, and its distribution is illustrated in Fig. 4(a) in which σ_{su} , σ_{sf} and σ_c are the normal stresses in the steel tube, in the bottom flat-plate flange and in the infilled concrete respectively. σ_{su} , σ_{sf} and σ_c are linearly distributed along the flange height to the neutral axis. The transverse normal stress, as shown in Fig. 4(b), is produced due to the shear stress in the corrugated web. The shear stress in the connection between the thin-walled corrugated web and the flanges can be illustrated in Fig. 5. The shear force in any straight segment is in the length direction to form transverse bending moment M_t to the flanges. Under such transverse bending moment, transverse normal stress varies linearly along the width of the flanges as shown in Fig. 4(b).

Theoretical equations for calculating the in-plane normal stresses in the flanges of the new I-girder were presented by Shao and Wang (2017) as follows

$$\sigma'_s = \frac{M_x y}{(I_{st} + I_{sc}) + E_c/E_s \cdot I_{cc}} = \frac{M_x y}{I_e} \quad (1)$$

$$\sigma'_c = \frac{M_x y}{E_s/E_c \cdot (I_{st} + I_{sc}) + I_{cc}} = \frac{M_x y}{E_s/E_c \cdot I_e} \quad (2)$$

where σ'_s and σ'_c are the in-plane normal stresses in the steel and in the concrete respectively; E_s and E_c are the elastic modulus of the steel and the elastic modulus of the concrete respectively; I_e is the equivalent moment of inertia of the cross section, and $I_e = (I_{st} + I_{sc}) + E_c/E_s \cdot I_{cc}$; I_{st} , I_{sc} and I_{cc} are the moments of inertia for the bottom flat-plate flange, for

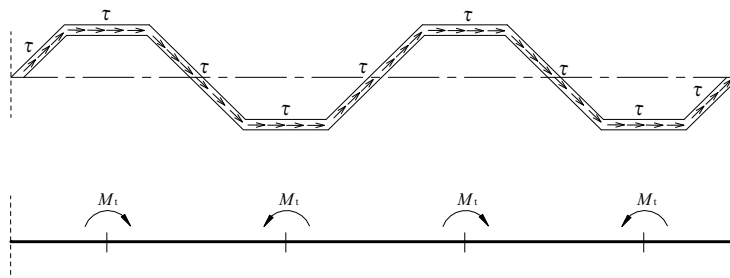


Fig. 5 Shear stress flow in the corrugated web

the top tube and for the concrete respectively; M_x is the in-plane bending moment; y is the distance of the stress location in the flange to the neutral axis.

The moments of inertia of the steel and of the concrete are calculated from the following equation (Shao and Wang 2017)

$$\left\{ \begin{array}{l} I_{st} = b_{f2} \cdot t_f \cdot y_n^2 \\ I_{sc} = \frac{1}{12} \left[b_{f1} \cdot h_u^3 - (b_{f1} - 2t_u)(h_u - 2t_u)^3 \right] \\ \quad + 2t_u \cdot (b_{f1} + h_u) \left(H - y_n - \frac{h_u}{2} \right)^2 \\ I_{cc} = \frac{1}{12} (b_{f1} - 2t_u)(h_u - 2t_u)^3 \\ \quad + (b_{f1} - 2t_u)(h_u - 2t_u) \left(H - y_n - \frac{h_u}{2} \right)^2 \end{array} \right. \quad (3)$$

where b_{f1} and b_{f2} are the widths of the top concrete-filled tubular flange and the bottom flat-plate flange respectively; H is the height of the new I-girder; h_u and t_u are the height and the thickness of the top tubular flange respectively; t_f is the thickness of the bottom flat-plate flange; y_n is the distance of the bottom flat-plate to the neutral axis.

To calculate the in-plane normal stress through Eqs. (1)-(2), the neutral axis on the cross section is necessary to be determined. Shao and Wang (2017) presented the following equation to determine the location of such neutral axis through the calculation of y_n as follow

$$y_n = \frac{A_{f1} \cdot (H - h_u / 2)}{A_{f1} + A_{f2}} \quad (4)$$

where A_{f1} and A_{f2} are equivalent areas of the top and the bottom flanges respectively.

A_{f1} and A_{f2} are calculated from the following equations

$$\left\{ \begin{array}{l} A_{f1} = A_{sc} + E_c / E_s \cdot A_{cc} \\ A_{f2} = b_{f2} t_f \end{array} \right. \quad (5)$$

where $A_{sc} = 2t_u(b_{f1} + h_u - 2t_u)$, $A_{cc} = (b_{f1} - 2t_u)(h_u - 2t_u)$.

The transverse normal stress is calculated based on the known transverse bending moment M_t in the flanges. Abbas *et al.* (2007a, b) provided the calculation of M_t from a fictitious load method as follow

$$M_t = \frac{2V_y}{H} \left(-A^{trap} + \xi A_L \right) \quad (6)$$

where V_y is the shear force at the given cross section, A^{trap} is the accumulated area under the corrugation profile as shown in Fig. 6; A_L is the accumulated area under the corrugation profile along the entire span of the I-girder; ξ is a ratio of the given length to the span, i.e., $\xi = z/L$ (z is the distance to the girder's end in the length direction of the girder, and L is

the girder's length).

Once the transverse bending moment M_t is determined from Eq. (6), the transverse normal stresses in the top concrete-filled tubular flange are then calculated from the following equations

$$\sigma_{sc}'' = \frac{M_t x}{I_{ts1} + E_c / E_s \cdot I_{tc}} = \frac{M_t x}{I_{te}} \quad (7)$$

$$\sigma_{cc}'' = \frac{M_t x}{E_s / E_c \cdot I_{ts1} + I_{tc}} = \frac{M_t x}{E_s / E_c \cdot I_{te}} \quad (8)$$

where σ_{sc}'' and σ_{cc}'' are the transverse normal stresses in the steel tube and in the concrete respectively; I_{ts1} and I_{tc} are the moments of inertia for the steel tube and for the concrete respectively; I_{te} is the equivalent moment of inertia for the concrete-filled tubular flange, and $I_{te} = I_{ts1} + E_c / E_s \cdot I_{tc}$.

The transverse normal stress in the bottom flat-plate flange is calculated from the following equation

$$\sigma_{st}'' = \frac{M_t x}{I_{ts2}} \quad (9)$$

where $I_{ts1} = t_f b_{f2}^3 / 12$.

Based on Eqs. (1)-(2), (7)-(9), the normal stresses in the steel tube (σ_{sc}), in the concrete (σ_{cc}) and in the bottom flat-plate flange (σ_{st}) can be calculated from the following equation

$$\left\{ \begin{array}{l} \sigma_{sc} = \sigma_s' + \sigma_{sc}'' = \frac{M_x y}{I_e} + \frac{M_t x}{I_{te}} \\ \sigma_{cc} = \sigma_c' + \sigma_{cc}'' = \frac{E_c}{E_s} \left(\frac{M_x y}{I_e} + \frac{M_t x}{I_{te}} \right) \\ \sigma_{st} = \sigma_s' + \sigma_{st}'' = \frac{M_x y}{I_e} + \frac{M_t x}{I_{ts2}} \end{array} \right. \quad (10)$$

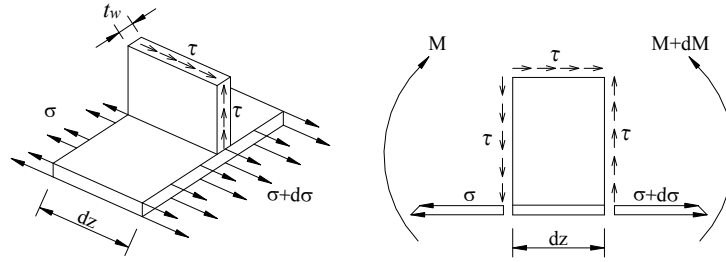
2.3 Shear stress in the corrugated web

According to the assumptions (4) and (5) in Section 2.1, the corrugated web sustains only shear force while the bottom flat-plate flange only sustains normal stress. An infinitesimal segment of the new I-girder in the length direction is taken for analysis, and the shear stress at a position on the corrugated web with a distance of y to the bottom flange is shown in Figs. 7(a) and (b). When the position is located at the straight segment of the trapezoidal web as shown in Fig. 7(a), the force equilibrium in the length direction produces the following equation

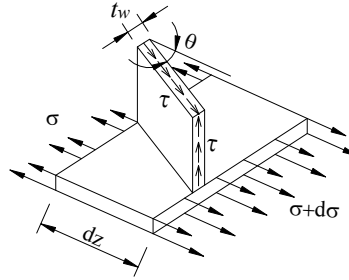
$$\tau \cdot t_w \cdot dz = \int_{A_{f2}} \frac{dM_x}{I_e} y dA \quad (11)$$

The shear stress is then calculated from the following equation

$$\tau = \frac{1}{t_w I_e} \int_{A_{f2}} \frac{dM_x}{dz} y dA = \frac{V_y}{t_w I_e} \int_{A_{f2}} y dA \approx \frac{V_y A_{f2} y_n}{t_w I_e} \quad (12)$$



(a) Shear stress in the straight segment of the corrugated web



(b) Shear stress in the inclined segment of the corrugated web

Fig. 7 Shear stress in the corrugated web

where t_w is the thickness of the corrugated web.

If an equivalent area A_{we} is denoted as follow

$$A_{we} = \frac{t_w I_e}{A_{f2} y_n} \quad (13)$$

Then, Eq. (12) can be expressed as follow

$$\tau = \frac{V_y}{A_{we}} \quad (14)$$

As it is easy to see from Eq. (13) that A_{we} is a constant for a given new I-girder, the shear stress on the cross section in the straight segment of the corrugated web is uniform.

The shear stress in the inclined segment of the corrugated web can be also calculated from similar method. As seen from Fig. 7(b), the force equilibrium in the length direction is expressed as follow

$$\begin{aligned} \tau \cdot A \cdot \cos \theta &= \tau \cdot t_w \cdot \frac{dz}{\cos \theta} \cdot \cos \theta \\ &= \tau \cdot t_w \cdot dz = \int_{A_{f2}} \frac{dM_x}{I_e} y dA \end{aligned} \quad (15)$$

Obviously, the force equilibrium of the inclined segment in length direction of the new I-girder is identical to Eq. (11). Therefore, Eq. (14) is also applicable for calculating the shear stress in the inclined segment of the corrugated web.

The shear force sustained by the corrugated web is calculated from the following equation

$$V_y^{cor} = \tau \cdot A_w = \frac{V_y}{A_{we}} \cdot t_w \cdot (H - h_u - t_f) \quad (16)$$

$$\approx \frac{V_y A_{f2} y_n (H - h_u)}{I_e} \quad (16)$$

Therefore, the percentage of shear forced sustained by the corrugated web is estimated from the following equation

$$\eta = \frac{V_y^{cor}}{V_y} = \frac{A_{f2} y_n (H - h_u)}{I_e} \quad (17)$$

When η is not very close to 1.0, the top concrete-filled tubular flange also sustains some amount of shear force in the new I-girder, which indicates that it is not suitable to assume that the corrugated web sustains most of the shear force.

3. Verification of theoretical equations

3.1 Experimental tests

To verify the accuracy of the presented equations for calculating the normal and the shear stresses in the new I-girder, a reliable method is to compare the stresses predicted from the equations with experimental results obtained from tests. Overall two specimens were tested, and the normal stresses and the shear stresses at some selected positions were obtained from the experimental tests. The corrugated webs used in the specimens are fabricated with flat-plates of 3 mm in thickness. The flat plate was cold-formed to be corrugated web in factory according to the designed dimensions.

The first specimen was a simply supported girder with a span of 6 m, and it was introduced by Shao and Wang (2017). The new I-girder specimen before filling concrete in the top tubular flange and the testing scheme are illustrated in Fig. 8. Detailed dimensions can be found in the reported

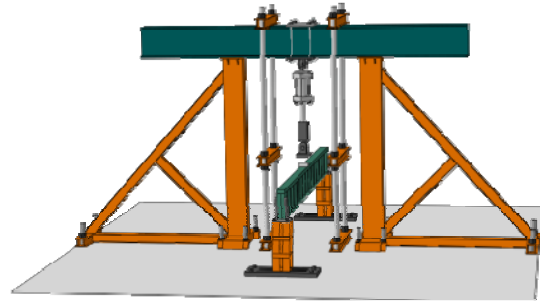


Fig. 8 Specimen of I-girder with a span of 6m and test rig

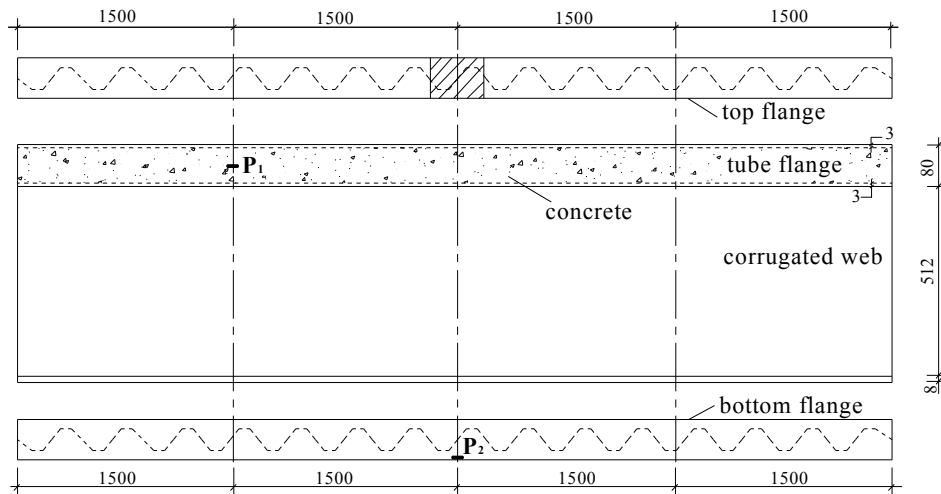


Fig. 9 Two selected locations P1 and P2 in SP1

Table 1 Dimensions of specimen SP2

H (mm)	L (mm)	b_f (mm)	h_u (mm)	t_f (mm)	t_u (mm)	t_w (mm)	b (mm)	d (mm)	h (mm)	θ ($^\circ$)
600	2186	120	60	5	3	3	73	60	60	45

Table 2 Mechanical properties of steel materials

Part	Yielding strength (MPa)	Tensile strength (MPa)	Elastic modulus (GPa)	Elongation
Web (3 mm)	341	473	208	21%
Flat-plate flange (5 mm)	318	481	201	22%
Steel tube (3 mm)	350	419	208	13.6%

work by Shao and Wang (2017). The specimen, named as SP1, was hinged at both ends on two supports. A concentrated load was applied at the mid-span to produce both shear force and bending moment on the cross section at any given location along the length.

During the loading process, the normal strains at two selected locations, namely P1 and P2, were measured through placed strain gauges as shown in Fig. 9. P1 was located at the mid-height of the side wall of the top tubular flange, and the distance of P1 to the left end of the specimen was 1/4 of the span. P2 was located at the mid span of the bottom flat-plate flange. The strain gauges were placed in the longitudinal direction of the specimen to

measure the normal strains of the top and the bottom flanges.

As the shear strain in the web was not measured during the test for specimen SP1, another specimen with a short span, named as SP2, was also tested. The geometry of specimen SP2 is shown in Fig. 10. The detailed dimensions of specimen SP2 are listed in Table 1. In SP2, the widths of the top concrete-filled tubular flange and the bottom flat-plate flange are identical, i.e., $b_{f1} = b_{f2} = b_f$.

The mechanical properties of the steel materials used in specimen SP2 were measured from uni-axial tensile tests for standard coupons. The yield strength, the tensile strength, the elastic modulus and the elongation percentage

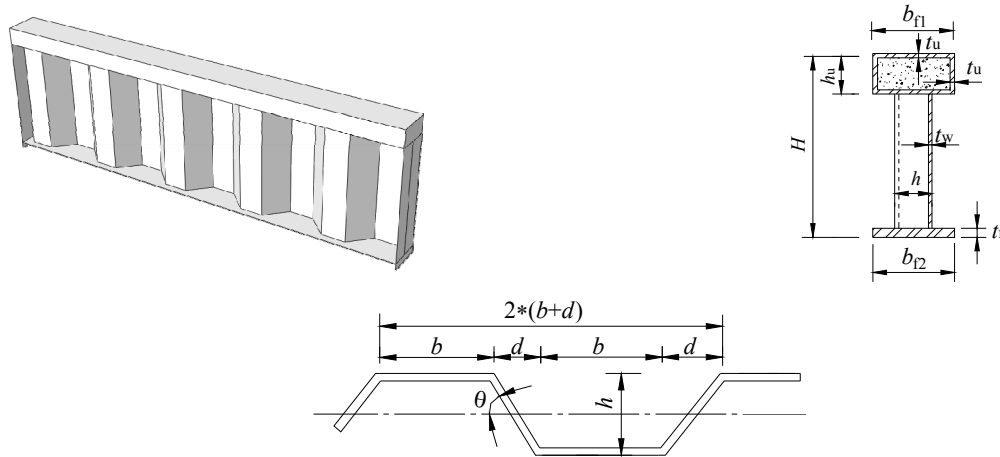


Fig. 10 Geometry of specimen SP2

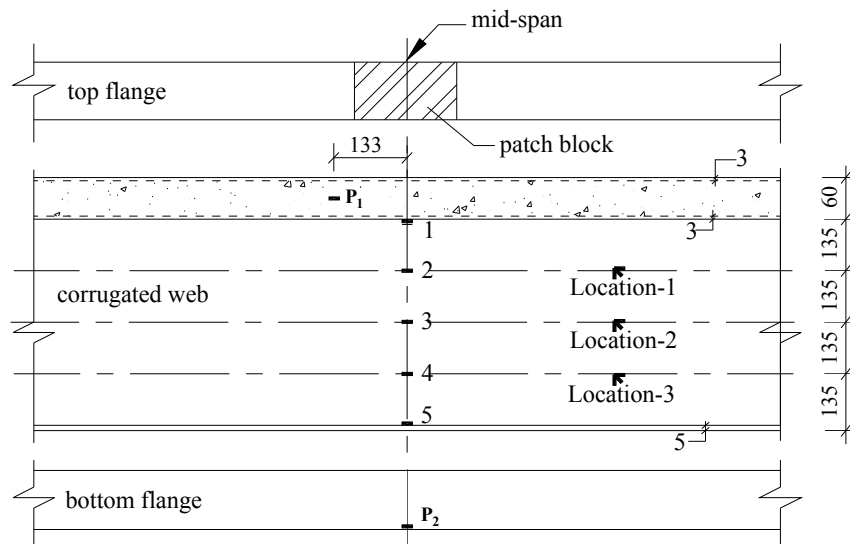


Fig. 11 Placement of strain gauges

were all obtained from the measured stress-strain curve, and they are tabulated in Table 2. The compressive strength and the elastic modulus of the infilled concrete were measured from the compressive test for standard cubic concrete specimens after a curing period of a month. The characteristic compressive strength of the concrete is 30.2 MPa and the elastic modulus is 30 GPa.

Some strain gauges were placed on the flanges and on the corrugated web to measure the normal strain and the shear strain. The placement of strain gauges was illustrated in Fig. 11. Two strain gauges were placed in P1 and P2 to measure the normal stresses in the top flange and in the bottom flange respectively. Five strain gauges (1, 2, 3, 4 and 5 in Fig. 11) were placed uniformly along the web height at the mid-span, and the direction of the five strain gauges is in the length of the girder. These five strain gauges were used to measure the normal strain in the web and hence to verify the so-called accordion effect in the corrugated web. Three strain rosettes were placed uniformly in the web as seen in Fig. 11 to measure the shear strain at the three locations (Location 1, Location 2 and Location 3). Detailed

calculation of the shear strain will be discussed later.

In the experimental test, SP2 was supported at both ends through pin connection as shown in Fig. 12. A concentrated load was applied at the mid-span on the top tubular flange to produce shear force and bending moment on the cross section of the specimen. The concentrated load was increased with a specified increment through the actuator till the failure of SP2. The failure mode of SP2 was observed from Fig. 12. It is clear that a large flexural deformation occurs when the specimen fails finally although the span of SP2 is very short compared to the height of the girder. Due to the so-called accordion effect of the corrugated web, the top and the bottom flanges sustain almost all of the bending moment. The two flanges can be simplified into two independent beams and the corrugated web provides lateral supports to them.

After failure, a clear in-plane bending deformation is observed in the top concrete-filled tubular flange as shown in Fig. 12(b). However, the transverse flexural deformation is almost invisible, as shown in Fig. 13(a). For the bottom flat-plate flange, both in-plane and transverse flexural

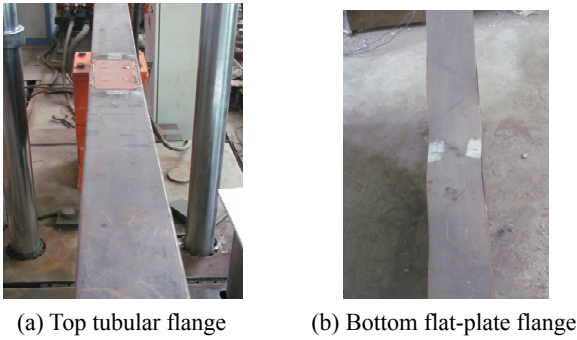


Fig. 13 Deformation of flanges

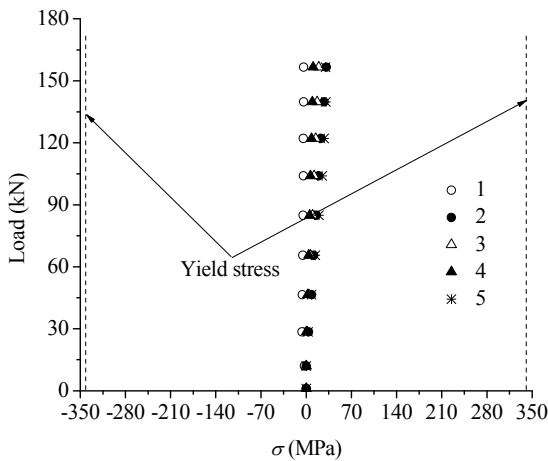


Fig. 14 Normal stress development on the web

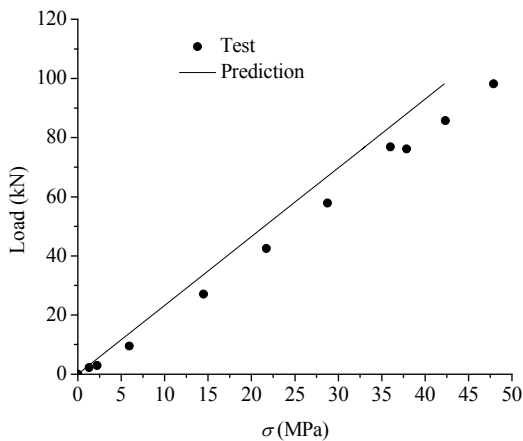
deformations can be observed clearly, as shown in Fig. 12(b) and 13(b). The transverse residual deformation proves the existence of the transverse normal stress, and its effect on the final failure mode seems to be not negligible.

3.2 Verification of normal stress

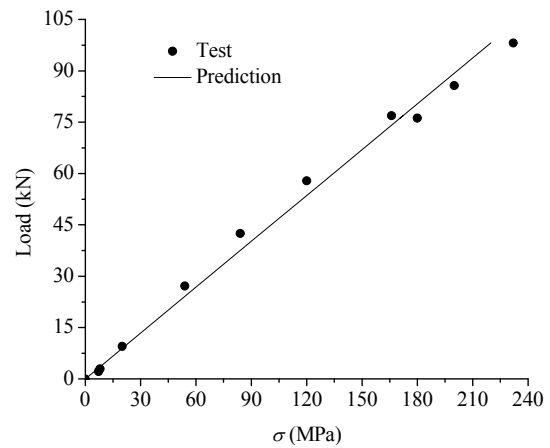
As mentioned previously, the corrugated web is assumed to have no contribution to the normal stress

produced by the bending moment due to the accordion effect. This assumption was already verified from many reported tested results in the literature. In this study, it can be still verified through the measured normal strains on the web. Fig. 14 shows the normal stress (σ) development along the web height at the mid-span (five positions 1, 2, 3, 4 and 5) with the increase of the concentrated load for specimen SP2. All the normal stresses are very minor and far away from the yield stress of the web (341 MPa) before final failure of SP2 (the measured yielding load is about 220 kN), which is coincident with previous reported results.

The normal stress ν in the flanges of SP1 and SP2 for both specimens can be calculated from Eq. (10) in theory. Based on the measured normal strain ϵ in the experimental tests, the normal stress σ can be also obtained from Hooke's law ($\sigma = E\epsilon$). The predicted normal stresses from Eq. (10) and the experimentally measured values at two selected locations P1 and P2 for specimens SP1 and SP2 are plotted together in Figs. 15-16. For specimen SP1, the predicted normal stress at P2 has a better agreement with experimental measurement compared to the predicted result at P1. P2 is a location on the surface of the bottom flat-plate flange while P1 is located at the side wall of the top steel tube of the tubular flange. The predicted normal stress at P1 seems not to agree well with the experimental result. It may be due to the following reasons: (1) The steel tube has a much smaller wall thickness, and imperfection of the tube wall may produce additional bending stress when the top tubular flange is under compression. (2) The tubular flange is relatively longer, and it is not easy to assure that the infilled concrete has absolute adhesion to the steel tube. Hence, the steel tube may not cooperate with the infilled concrete perfectly. For specimen SP2, the strain gauge placed at P1 peeled off at a small loading. Therefore, the measured normal stress development at P1 in the top tubular flange does not have a long stage. In overall, the stress development predicted from Eq. (10) is in satisfactory agreement with experimental result for the specimens SP1 and SP2, which indicates that Eq. (10) can produce reasonably accurate estimation on the normal stress in the flanges of the new I-girder.



(a) Location P₁



(b) Location P₂

Fig. 15 Comparison of stress development in locations P₁ and P₂ for SP1

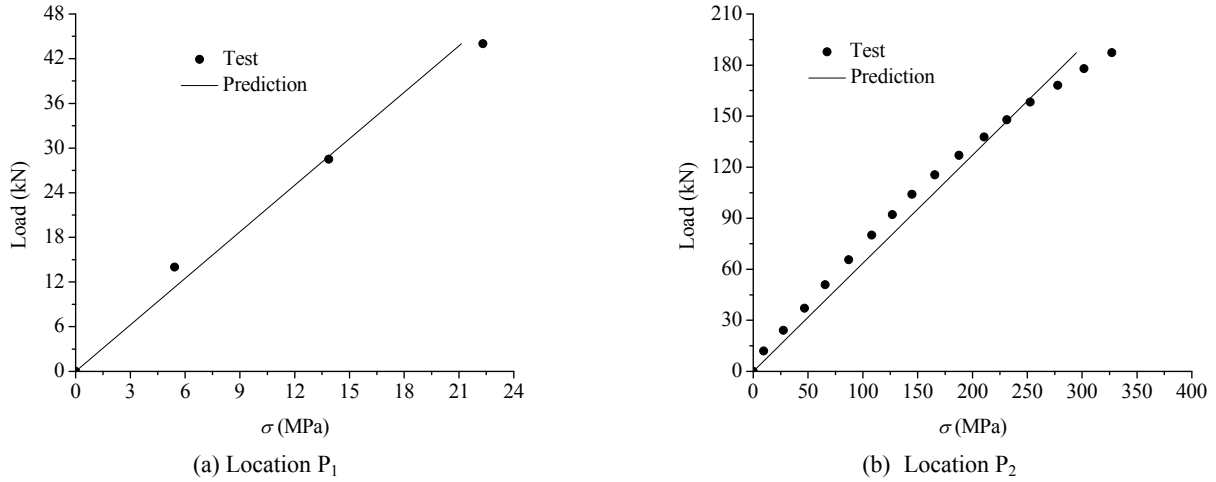


Fig. 16 Comparison of normal stress development in locations P₁ and P₂ for SP2

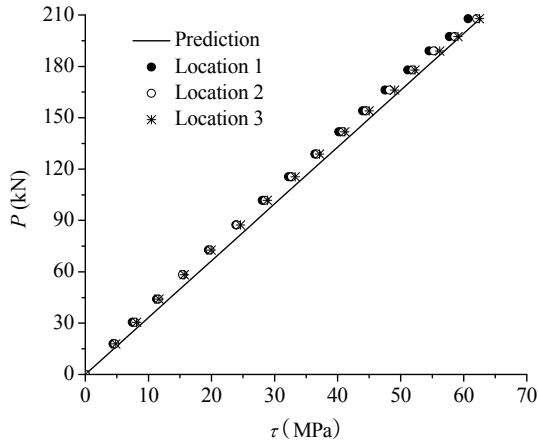


Fig. 17 Comparison of shear stress on the web for SP2

3.3 Verification of shear stress

The shear stress development on the corrugated web in the experimental test for SP2 can be obtained from the measured strains from the three strain rosettes as shown in Fig. 11. In each strain rosette, three strain gauges are placed to measure the strains in horizontal direction (ε_0), in an inclined direction with an angle of 45° (ε_{45}) and in vertical direction (ε_{90}) respectively. The shear strain γ is then calculated from the following equation

$$\gamma = 2\varepsilon_{45} - (\varepsilon_0 + \varepsilon_{90}) \quad (18)$$

After the shear strain γ is calculated, the shear stress on the web can be calculated directly from Hooke's law as follow

$$\tau = \frac{E}{2(1+\mu)}\gamma \quad (19)$$

where μ is Poisson's ratio, and its value is 0.3 in this study.

The experimentally measured shear stresses at the three locations are calculated from Eqs. (18)-(19). In theory, such shear stresses can be predicted from Eq. (14). Similarly, experimental and predicted results of the shear stress

development at three locations are plotted together in Fig. 17. Two conclusions can be drawn based on the results in Fig. 17: (1) Eq. (14) can produce accurate estimation on the shear stress in the corrugated web; (2) Shear stress in the corrugated web is uniform along the height of the web because the shear stresses at the three locations are almost same during the loading process.

From Eq. (17), the amount of shear force sustained by the corrugated web can be calculated. For SP2, the value of η is 93.8%. Similarly as conventional I-girder, the corrugated web in the new I-girder still sustains most of the shear force.

3.4 Prediction on flexural yielding strength

Eqs. (10) and (14) are verified to be accurate for estimating the normal stress in the flanges and the shear stress in the corrugated respectively in the above session. As the failure modes of the two specimens SP1 and SP2 are both flexural yielding, Eq. (10) can be used to predict the flexural yielding strength of the new I-girder. As it was found that yielding occurs firstly in the bottom flat-plate flange for both specimens, the following equation is satisfied at such yielding state

$$\sigma_y = \frac{M_x y}{I_e} + \frac{M_t x}{I_{ts2}} \quad (20)$$

where σ_y is the yielding strength of the steel material for the bottom flat-plate flange.

For specimen SP1, $\sigma_y = 252$ MPa, $M_x = FL/4$ (F is the concentrated load at the mid-span) and M_t is calculated from Eq. (6). The shear force is identical on any cross section along the span ($V_y = F/2$). Based on the above results, the yielding load F is calculated, and the result is 102 kN. Under this loading, the in-plane normal stress and the transverse normal stress in the bottom flat-plate flange are 211 MPa and 41 MPa respectively. The transverse normal stress is about 20% of the in-plane normal stress, and its effect on the overall normal stress cannot be ignored. The predicted yielding load is plotted in the load-deflection curve of SP1 obtained from experimental test as shown in

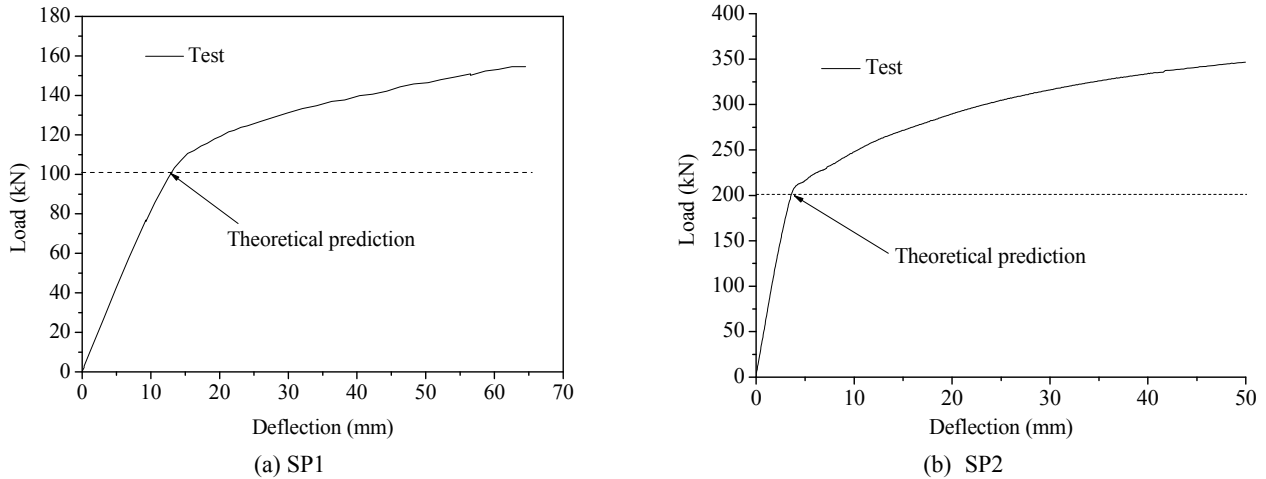


Fig. 18 Comparison of yielding load from theoretical prediction and experimental test

Fig. 18(a). It is noted here that the transverse normal stress was not considered in the reported work by Shao and Wang (2017). Similarly, the yielding load for SP2 can be also calculated by using the same method. For SP2, $\sigma_y = 318$ MPa. The transverse normal stress is zero at the failure location due to a zero accumulated area under the corrugation profile. The predicted yielding load is about 203 kN for SP2, and corresponding comparison between predicted and tested yielding loads is shown in Fig. 18(b).

It is clearly found that the predicted yielding loads for the two specimens agree with experiment results very well. The presented equation for calculating the normal stress in the flanges of the new I-girder is proved to be accurate and reliable.

4. Design method

4.1 Criterion

In the presented composite I-girder, the corrugated web is proved to have nearly no resistance to tension or compression. Therefore, the following criteria are assumed in the design:

- (1) The bending moment on any cross section of a composite I-girder is sustained independently by the flanges while the shear force is sustained by both the flanges and the corrugated web.
- (2) The neutral axis is necessary to be located at the corrugated web to make full use of the tensile strengths of the bottom flange and the compressive strength of the top concrete-filled tubular flange.
- (3) As the corrugated web has nearly no resistance to tension or compression, the development of the plastic region in the bottom flange is not considered because the thickness of the bottom flange is negligible compared to the height of the cross section. In another word, elastic limit is assumed to be the failure state of the composite I-girder.

4.2 Material selection

As the presented composite I-girder is consisted of steel and concrete materials, the optimized design is to ensure that the concrete fails later than the steel material. From Eqs. (1)-(2), the following equation is easily obtained

$$\frac{\sigma'_c}{\sigma'_s} \approx \frac{E_c}{E_s} \leq \frac{\sigma_c}{\sigma_y} \quad (21)$$

where σ_c is the compressive strength of concrete.

From Eq. (21), the concrete grade used in the composite I-girder can be determined from the required compressive strength (σ_c) as follow

$$\sigma_c \geq \frac{E_c}{E_s} \sigma_y \quad (22)$$

4.3 Flexural strength

The flexural strength of the presented composite I-girder is determined from the yielding strength of the steel materials of the flanges due to two reasons: (1) the corrugated web has nearly no resistance to tension or compression caused by the bending of the I-girder; (2) the concrete in the steel tube fails no earlier than the steel materials. Hence, the flexural strength is determined from the following equations

$$\max \left(\frac{M_x y_n}{I_e} + \frac{M_t \cdot \frac{b_{f2}}{2}}{I_{te}}, \frac{M_x (H - y_n)}{I_e} + \frac{M_t \cdot \frac{b_{f1}}{2}}{I_{te}} \right) = \sigma_y \quad (23)$$

4.4 Shear strength

The shear force on the cross section of the composite I-girder is sustained by both the flanges and the corrugated web. The shear stress in the corrugated web is larger than

that in the flanges, and the shear strength is then determined from the maximum shear stress in the web as follow

$$\frac{V_y}{A_{we}} = f_v = \frac{\sigma_v}{\sqrt{3}} \quad (24)$$

where f_v is the shear strength of the steel material.

Eq. (24) is only used to evaluate the yielding of the corrugated web. If the corrugated web fails due to buckling, the design equation can be found from corresponding reported studies, such as Sause and Braxtan (2011).

5. Conclusions

Theoretical analysis for calculating the stress in an I-girder with top concrete-filled tubular flange and corrugated web is presented. The accuracy of the presented method is verified through comparing theoretical prediction with experimental result. Based on the conducted work, the following three conclusions can be drawn:

- (1) Almost all of the normal stresses are sustained by the flanges in the new I-girder while most of the shear stresses are undertaken by the corrugated web.
- (2) The normal stresses in the top and the bottom flanges are consisted of both in-plane component and transverse component. The transverse normal stress may produce significant effect on the failure state of the bottom flat-plate flange.
- (3) The shear stress distribution along the web height is uniform.

References

- Abbas, H.H., Sause, R. and Driver, R.G. (2006), "Behavior of corrugated web I-girders under in-plane loads", *J. Eng. Mech.*, **132**(8), 806-814.
- Abbas, H.H., Sause, R. and Driver, R.G. (2007a), "Analysis of flange transverse bending of corrugated web I-girders under in-plane loads", *J. Struct. Eng.*, **133**(3), 347-355.
- Abbas, H.H., Sause, R. and Driver, R.G. (2007b), "Simplified analysis of flange transverse bending of corrugated web I-girders under in-plane moment and shear", *Eng. Struct.*, **29**(11), 2816-2824.
- Anapayan, T., Mahendran, M. and Mahaarachchi, D. (2011), "Lateral distortional buckling tests of a new hollow flange channel beam", *Thin-Wall. Struct.*, **49**(1), 13-25.
- Avery, P. and Mahendran, M. (1997), "Finite-element analysis of hollow flange beams with web stiffeners", *J. Struct. Eng.*, **123**(9), 1123-1129.
- Barakat, S., Mansouri, A.A. and Altoubat, S. (2015), "Shear strength of steel beams with trapezoidal corrugated webs using regression analysis", *Steel Compos. Struct., Int. J.*, **18**(3), 757-773.
- Chen, X.C., Au, F.T.K., Bai, Z.Z., Li, Z.H. and Jiang, R.J. (2015), "Flexural ductility of reinforced and prestressed concrete sections with corrugated steel webs", *Comput. Concrete, Int. J.*, **16**(4), 625-642.
- Elgaaly, M., Hamilton, R.W. and Seshadri, A. (1996), "Shear strength of beams with corrugated webs", *J. Struct. Eng.*, **122**(4), 390-398.
- Elgaaly, M., Seshadri, A. and Hamilton, R.W. (1997), "Bending strength of steel beams with corrugated webs", *J. Struct. Eng.*, **123**(6), 772-782.
- Gao, F., Zhu, H.P., Zhang, D.H. and Fang, T.S. (2014), "Experimental investigation on flexural behavior of concrete-filled pentagonal flange beam under concentrated loading", *Thin-Wall. Struct.*, **84**, 214-225.
- Hassanein, M.F. and Kharoob, O.F. (2010), "Shear strength and behavior of transversely stiffened tubular flange plate girders", *Eng. Struct.*, **32**, 2617-2630.
- Hassanein, M.F. and Silvestre, N. (2013), "Lateral-distortional buckling of hollow tubular flange plate girders with slender unstiffened webs", *Eng. Struct.*, **56**, 572-584.
- Hassanein, M.F., Kharoob, O.F. and El Hadidy, A.M. (2013), "Lateral-torsional buckling of hollow tubular flange plate girders with slender stiffened webs", *Thin-Wall. Struct.*, **65**, 49-61.
- He, J., Liu, Y.Q., Xu, X.Q. and Li, L.B. (2014), "Load capacity evaluation of composite box girder with corrugated webs and steel tube slab", *Struct. Eng. Mech., Int. J.*, **50**(4), 501-524.
- Kalali, H., Hajsadeghi, M., Zirakian, T. and Alaei, F.J. (2015), "Hysteretic performance of SPSPs with trapezoidally horizontal corrugated web-plates", *Steel Compos. Struct., Int. J.*, **19**(2), 277-292.
- Kim, B.G. and Sause, R. (2008), "Lateral torsional buckling strength of tubular flange girders", *J. Struct. Eng.*, **134**(6), 902-910.
- Kim, B.G., Wimer, M.R. and Sause, R. (2005), "Concrete-filled rectangular tubular flange girders with flat or corrugated webs", *Int. J. Steel Struct.*, **5**, 337-348.
- Kövesdi, B., Jäger, B. and Dunai, L. (2012), "Stress distribution in the flanges of girders with corrugated webs", *J. Constr. Steel Res.*, **79**, 204-215.
- Mahendran, M. and Avery, P. (1997), "Buckling experiments on hollow flange beams with web stiffeners", *J. Struct. Eng.*, **123**(9), 1130-1134.
- Nie, J.G., Zhu, L., Tao, M.X. and Tang, L. (2013), "Shear strength of trapezoidal corrugated steel webs", *J. Constr. Steel Res.*, **85**, 105-115.
- Pi, Y.L. and Trahair, N.S. (1997), "Lateral-distortional buckling of hollow flange beams", *J. Struct. Eng.*, **123**(6), 695-702.
- Sause, R. (2015), "Innovative steel bridge girders with tubular flanges", *Struct. Infrastruct. Eng.*, **11**(4), 450-465.
- Sause, R. and Braxtan, T.N. (2011), "Shear strength of trapezoidal corrugated steel webs", *J. Struct. Eng.*, **67**, 223-236.
- Sause, R., Kim, B.G. and Wimer, M.R. (2008), "Experimental study of tubular flange girders", *J. Struct. Eng.*, **134**(3), 384-392.
- Shao, Y.B. and Wang, Y.M. (2016), "Experimental study on shear behavior of I-girder with concrete-filled tubular flange and corrugated web", *Steel Compos. Struct., Int. J.*, **22**(6), 1465-1486.
- Shao, Y.B. and Wang, Y.M. (2017), "Experimental study on static behavior of I-girder with concrete-filled rectangular flange and corrugated web under concentrate load at mid-span", *Eng. Struct.*, **130**, 124-141.
- Zhao, X.L. and Mahendran, M. (1998), "Recent innovations in cold-formed tubular sections", *J. Constr. Steel Res.*, **46**(1-3), 472-473.